Composition of Ge(Si) islands in the growth of Ge on Si(111) by x-ray spectromicroscopy

Fulvio Ratto and Federico Rosei[a)]
Institut National de la Recherche Scientifique-Energie, Materiaux et Telecommunications (INRS-EMT), Université du Quebec, 1650 Boulevard Lionel Boulet, J3X 1S2 Varennes (Quebec) Canada

Andrea Locatelli, Salia Cherifi, Stefano Fontana, and Stefan Heun[b)]
Sincrotrone Trieste S.C.p.A., S.S. 14 Km 163.5, 34012 Trieste, Italy

Pierre-David Szkutnik, Anna Sgarlata, and Maurizio De Crescenzi
Dipartimento di Fisica and Unità Istituto Nazionale per la Fisica della Materia (INFM), Università di Roma II, Via della Ricerca Scientifica n.1, 00133 Roma, Italy

Nunzio Motta
Dipartimento di Fisica and Unità Istituto Nazionale per la Fisica della Materia (INFM), Università di Roma TRE, Via della Vasca Navale 84, 00100 Roma, Italy

(Received 3 August 2004; accepted 19 October 2004; published online 24 January 2005)

The stoichiometry of Ge/Si islands grown on Si(111) substrates at temperatures ranging from 460 to 560 °C was investigated by x-ray photoemission electron microscopy (XPEEM). By developing a specific analytical framework, quantitative information on the surface Ge/Si stoichiometry was extracted from laterally resolved XPEEM Si 2*p* and Ge 3*d* spectra, exploiting the chemical sensitivity of the technique. Our data show the existence of a correlation between the base area of the self-assembled islands and their average surface Si content: the larger the lateral dimensions of the 3D structures, the higher their relative Si concentration. The deposition temperature determines the characteristics of this relation, pointing to the thermal activation of kinetic diffusion processes. © *2005 American Institute of Physics*. [DOI: 10.1063/1.1832747]

I. INTRODUCTION

The heteroepitaxial growth of group IV semiconductors is presently a subject of great interest due to the possibility it offers to engineer and tailor electronic components according to the technological needs. In particular, the ability to control the self-assembly processes of Ge/Si nanostructures on silicon surfaces will hopefully lead to the integration of microelectronic and optoelectronic devices on the same Si chip.[1–3]

It is well known that the growth of Ge on Si(111) in the temperature range of 400–700 °C can be described as a *modified* Stranski–Krastanov (SK) process, where the onset of three-dimensional (3D) Ge/Si islanding follows the formation of a uniform wetting layer (WL). The 4.2% lattice-parameter mismatch between Si and Ge leads to surface roughening and islanding, when the germanium coverage exceeds a critical value of ~3–5 monolayers (ML), depending on substrate temperature and growth rate. The subsequent nucleation of 3D islands represents an intriguing phenomenon, both from a scientific point of view and for possible applications. The carrier confining properties of these nanostructures may pave the road to the fabrication of quantum dot (QD)-based devices with a vast range of applications, from light emitters to biosensors to quantum computers. Moreover, Ge/Si nanostructures grown on Si surfaces may be easily integrated with the existing silicon-based technology, with obvious economic advantages.

Most of the geometric and thermodynamic features both of individual and of statistical ensembles of 3D islands, together with the ultimate electronic properties of the system, strongly depend on the surface local chemical composition and stoichiometry. Intermixing and alloying allow the accumulated strain energy in the system to be partially released, and are known to occur starting with the very first stages of Ge deposition on Si,[4,5] even at relatively low growth temperatures.[6] The Si/Ge concentration profile in single 3D islands is presently the focus of many experimental reports, aimed at the description of the structural and electronic properties of the dots. Many groups have attempted to elucidate the dynamics of alloying in individual islands in related systems, by means of cross-sectional techniques, such as scanning tunneling microscopy[7] (STM) or transmission electron microscopy (TEM).[8–13] However, the preparation of a cross-sectional specimen may easily alter or damage the sample. On the other hand, little is known about the lateral in-plane intermixing gradient, hindering an understanding of the fundamental diffusion processes that lead to the alloying itself. This topic is highly controversial and alternative models, based either on thermodynamic[14,15] or kinetic[7,14,16,17] considerations, have been proposed to describe the existing experimental results. Presently, a unique picture of the phenomenon is not available, and the experimental evidence, based on the cross-sectional observations alone, is not conclusive.

[a)]Author to whom correspondence should be addressed; electronic mail: rosei@inrs-emt.uquebec.ca
[b)]Author to whom correspondence should be addressed; present address: Laboratorio Nazionale TASC, Area Science Park, S.S. 14 Km 163.5, Basovizza-34012 Trieste, Italy; electronic mail: heun@tasc.infm.it

In this article we report the combined results of low-energy electron microscopy (LEEM) and x-ray photoemission electron microscopy (XPEEM) experiments performed *in situ* on Ge/Si nanostructures grown on Si(111). Our measurements produced a two-dimensional (2D) "top view" mapping of the Si/Ge concentration distribution in the topmost surface layers, thus offering a complementary viewpoint to existing cross-sectional data. In a recent letter we have outlined the central findings of our preliminary XPEEM results.[18] Here we provide a detailed description of the experimental and analytical procedures that we developed in order to extract quantitative information from Ge/Si XPEEM spectra.

II. EXPERIMENT

The experiments were carried out using the spectroscopic photoemission and low-energy electron microscope (SPELEEM) at the nanospectroscopy beam line, which is available at the *Elettra* synchrotron facility in Trieste, Italy. The microscope allows LEEM and energy-filtered XPEEM measurements to be taken. Using low-energy electrons or x-ray synchrotron radiation as the probe, the microscope produces direct images of the surface after collecting and magnifying the electron (or photoelectron) flux emitted from the sample. A detailed description of the beam line and the experimental chamber can be found elsewhere.[19–21]

Under LEEM operating conditions, the surface can be imaged with a lateral resolution of ~10 nm and a time resolution of few tens of milliseconds. For the imaging of Ge growth, the microscope was operated in a bright-field mode. As a result, those portions of the island surface which are parallel to the substrate surface plane, i.e., the island tops and the WL, appear bright, in a sharp contrast with the highly stepped facets[22,23] at the sides of the Ge/Si islands.

The XPEEM measurements allow the acquisition of core-level photoelectron spectra with an energy resolution of ~0.25 eV and a lateral resolution of ~30 nm. The contrast in the resulting images is related to the chemical inhomogeneity of the surface. Due to the x-ray grazing incidence angle of 16°, the presence of 3D islands resulted in a partial shadowing of the WL. This effect was exploited to estimate the morphology of the surface in the vertical direction.

Si(111) samples were degassed for several hours at 600 °C and repeatedly flashed up to 1200 °C until a sharp 1×1 to 7×7 transition was observed while cooling the surface down to room temperature (RT).[24] Three different Si samples were prepared by depositing *in situ* 10 ML of Ge by molecular beam epitaxy (MBE) at a growth rate of ~0.2 ML/min, after stabilizing the sample temperature at 460, 530, and 560 °C, respectively. After cooling the surface to RT, the quality and morphology of the structures obtained were investigated by LEEM. Si2*p* and Ge3*d* XPEEM spectra were then acquired from randomly selected 3D islands in order to achieve representative statistics (the selected photon energy was 130.5 eV). Qualitatively, the contrast in the resulting spectral images is found to be associated with the relative local Si/Ge stoichiometry at the topmost layers of the grown systems.

III. QUANTITATIVE ANALYSIS OF XPEEM IMAGES AND SPECTRA

A correct interpretation of the contrast observed in the laterally resolved XPEEM images requires an adequate theoretical framework and system modeling. In the following we will discuss in detail the analytical procedure that we developed to quantitatively evaluate the local Ge/Si surface concentration.

We consider as our elemental photoelectron source an infinitesimal volume element dV of the sample with a Si concentration C_{Si} which is located at a depth h from the surface. If we assume the escape depth λ of the photoelectrons at a given kinetic energy to be essentially independent of the local Ge/Si stoichiometry, the measured Si2*p* photoelectron yield from the volume element dV can be expressed as[25]

$$dI \propto \Sigma_{\mathrm{Si}2p} C_{\mathrm{Si}} e^{-h/\lambda} dV. \tag{1}$$

Here, $\Sigma_{\mathrm{Si}2p}$ is the photoionization cross section of the Si2*p* core level at the selected photon energy. The proportionality factor accounts for all experimental parameters, such as local incident photon flux, detector acceptance solid angle, and selected integration time. In our case, the escape depth λ at the selected kinetic energies is on the order of 0.5 nm, which is much shorter than the photon attenuation length inside the sample. We can therefore assume that, within the volume from which the output signal dI is significant, the proportionality factor depends only on the coordinates $\mathbf{R}$ parallel to the surface plane.

The Si2*p* photoelectron yield at every point $\mathbf{R}$ on the sample surface is given by the integral of Eq. (1) along the coordinate z normal to the surface plane. It is convenient to explicitly write the spatial dependence of the Si concentration, $C_{\mathrm{Si}}(\mathbf{R},z)$. Referring to the sketch shown in Fig. 1, we hypothesize a profile of the form

$$C_{\mathrm{Si}}(\mathbf{R},z) = \begin{cases} C_{\mathrm{Si}}'(\mathbf{R}) & \text{for} \quad 0 \leqslant z < h^{i}(\mathbf{R}) \\ C_{\mathrm{Si}} & \text{for} \quad h^{i}(\mathbf{R}) \leqslant z < h^{wl}(\mathbf{R}) \\ 1 & \text{for} \quad z \geqslant h^{wl}(\mathbf{R}). \end{cases} \tag{2}$$

We have chosen the sample-vacuum interface as the origin of the z axis (directed towards the bulk of the sample) for every point $\mathbf{R}$. We have modeled the concentration profile as a step function with a constant stoichiometry inside the island and the WL at position $\mathbf{R}$. This is justified by the small value of the photoelectron escape depth. Only the electrons emitted by the uppermost surface layers escape from the surface and are collected by the microscope. Since our analysis procedure is meant to yield a value $C_{\mathrm{Si}}{}^{i}(\mathbf{R})$ for every island, our estimate has to be considered as an average over the first surface layers with the exponential weights $e^{-h/\lambda}$ defined in Eq. (1). We also assume that the WL Si concentration $C_{\mathrm{Si}}{}^{wl}$ and thickness $L^{wl}=h^{wl}(\mathbf{R})-h^{i}(\mathbf{R})$ are constant and independent of the position $\mathbf{R}$.

Integrating Eq. (1) over the z coordinate and using the $C_{\mathrm{Si}}(\mathbf{R},z)$ given in Eq. (2) yield a theoretical expression for the Si2*p* intensity $dI_{\mathrm{Si}}{}^{i}(\mathbf{R})$ collected from the island at position $\mathbf{R}$,

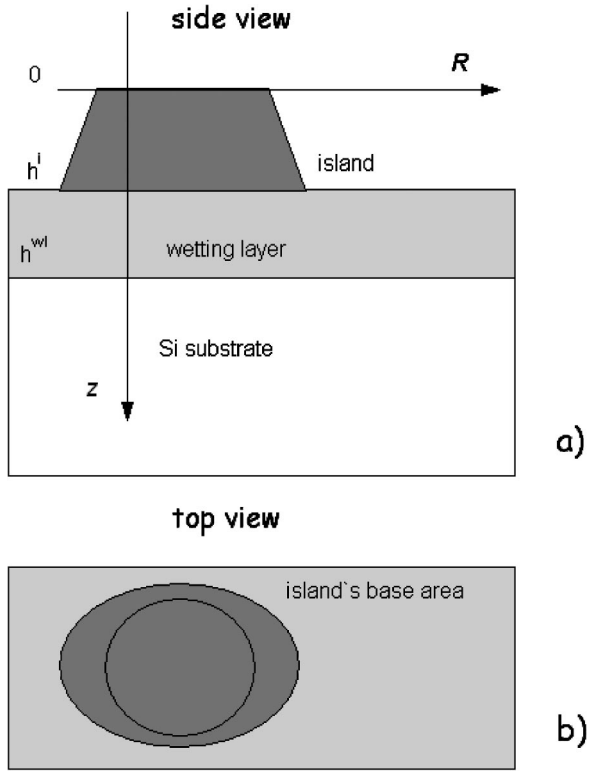

FIG. 1. Schematic representation of a portion of the sample with a modeled island: (a) side view and (b) top view.

$$dI_{\mathrm{Si}}{}^{i}(\mathbf{R}) \propto \Sigma_{\mathrm{Si}2p}\left\{\int_{0}^{h^{i}(\mathbf{R})} C_{\mathrm{Si}}{}^{i} e^{-z/\lambda} dz + \int_{h^{i}(\mathbf{R})}^{h^{i}(\mathbf{R})+L^{wl}} C_{\mathrm{Si}}{}^{wl} e^{-z/\lambda} dz + \int_{h^{i}(\mathbf{R})+L^{wl}}^{\infty} e^{-z/\lambda} dz\right\} dA$$
$$\propto \Sigma_{\mathrm{Si}2p}\lambda C_{\mathrm{Si}}{}^{i}(\mathbf{R})[1 + O(e^{-h^{i}(\mathbf{R})/\lambda})] dA. \quad (3)$$

In the second term of Eq. (3), we have explicitly listed the different contributions due to the island, the WL, and the Si substrate. In the following, terms of the order of $e^{-h^{i}(\mathbf{R})/\lambda}$ will be omitted, since the typical island height, as estimated by its XPEEM shadow length, is larger than 10 nm, thus the ratio $h^{i}(\mathbf{R})/\lambda$ is always larger than 20. The proportionality factor in Eq. (3) is related to the same experimental parameters as in Eq. (1). The infinitesimal area element of the surface region from which the intensity is collected, dA, corresponds to the lateral resolution of the microscope. Thus, the detected intensity corresponds to an average over any inhomogeneities in the sample stoichiometry within the area element dA. Furthermore, the variation in the surface x-ray illumination is negligible over an area much wider than the lateral resolution of the microscope.[20]

We can also calculate the Si2p photoemission yield from a region of the sample where no islands are present, by setting $h^{i}(\mathbf{R})=0$. Equation (4) models the photoelectron intensity emitted by that part of the surface covered by the WL only,

$$dI_{\mathrm{Si}}{}^{wl}(\mathbf{R}) \propto \Sigma_{\mathrm{Si}2p}\lambda\{C_{\mathrm{Si}}{}^{wl}[1 - e^{-(L^{wl}/\lambda)}] + e^{-(L^{wl}/\lambda)}\} dA. \quad (4)$$

Equations (3) and (4) represent the theoretical expressions for the Si2p intensity from the surface of a 3D island and from the WL, respectively. Thus, they can be directly used to fit the experimental data once the background intensity (mainly due to inelastically scattered electrons) is subtracted from the acquired spectra and images. To eliminate the proportionality factor related to the incident photon flux and acquisition parameters, we can introduce the ratio r_{Si} between the Si2p intensities from an island and from the surrounding WL. As a result, the infinitesimal area dA disappears from the formulas, leading to an equation that contains only experimentally accessible parameters,

$$r_{\mathrm{Si}}(\mathbf{R}) = \frac{C_{\mathrm{Si}}{}^{i}}{C_{\mathrm{Si}}{}^{wl}(1 - e^{-(L^{wl}/\lambda)}) + e^{-(L^{wl}/\lambda)}}. \quad (5)$$

The same procedure can be applied to analyze the Ge3d photoelectron peak. We will neglect the differences in the escape depths of the Si2p and Ge3d photoelectrons[26] and use the same symbol λ. Since the Ge concentration can be expressed as $C_{\mathrm{Ge}}(\mathbf{R},z)=1-C_{\mathrm{Si}}(\mathbf{R},z)$, we obtain

$$r_{\mathrm{Ge}}(\mathbf{R}) = \frac{1 - C_{\mathrm{Si}}{}^{i}}{(1 - C_{\mathrm{Si}}{}^{wl})[1 - e^{-(L^{wl}/\lambda)}]}. \quad (6)$$

Taking the Si2p and Ge3d XPEEM spectra acquired from the same region of the sample surface allows us to relate Eqs. (5) and (6) through the silicon surface concentration, thus obtaining the simple relation

$$C_{\mathrm{Si}}{}^{i} = \frac{r_{\mathrm{Ge}} - 1}{r_{\mathrm{Ge}}/r_{\mathrm{Si}} - 1}. \quad (7)$$

Again, r_{Si} is the ratio between the Si2p intensities emitted by the 3D island surface and the bare WL in its proximity, and r_{Ge} represents the analogous ratio measured for the Ge3d peak. Equation (7) can now be used to estimate the stoichiometry of the topmost layers of the individual islands under investigation, from the integration of the measured local Si2p and Ge3d spectra.

Figure 2 illustrates the procedure we have adopted to obtain the Si concentration in the islands. The measured values are intended as an average over the topmost layers, with the exponential weights $e^{-h/\lambda}$ in Eq. (1). We have summed images acquired at electron energies over a range corresponding to the Ge3d core level. This provides a micrograph whose contrast is roughly related to the local overall Ge3d photoelectron intensity and thus to the relative content of Ge (see the discussion of Fig. 3). In these micrographs, 3D islands can be clearly identified as bright areas on a dark background. The contrast in Fig. 2(a) is due to a stoichiometry gradient in the topmost layers. Our images demonstrate that the surfaces of the grown 3D structures are *enriched* in Ge with respect to the surrounding WL.

To examine this segregation phenomenon quantitatively, local photoelectron spectra are obtained from restricted areas in the image field of view, representing the island and the WL. Figures 2(b) and 2(c) show such spectra, which correspond to the average value of the photoelectron yield over the labeled regions of the micrograph in Fig. 2(a). After the background subtraction, the spectra integration yields the

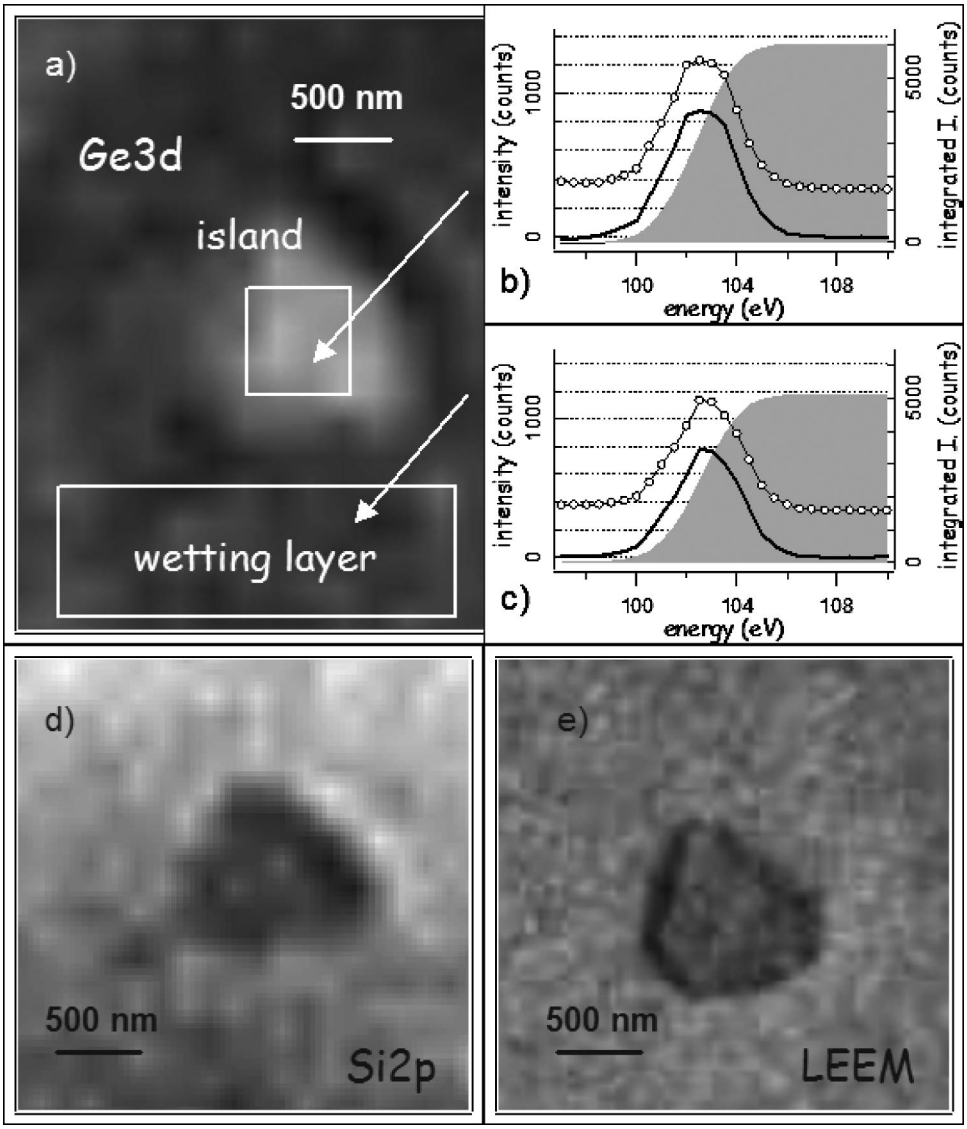

FIG. 2. (a): 2.5×3.4-μm^2 XPEEM image, integrated over the Ge3*d* photoelectron kinetic energies, displaying the typical island-wetting layer Ge3*d* contrast; (b) and (c): Ge3*d* photoelectron spectra, averaged over the regions labeled in (a): (b) from the top base of the 3D island, (c) from the wetting layer: circles: raw data; thick line: background-subtracted data; shadowed curve: overall intensity, used in the equations; (d): 2.8×2.8-μm^2 XPEEM image over the Si2*p* photoelectrons peak, displaying the same island shown in (a) as a dark structure on the bright wetting layer; and (e): 2.8×2.8-μm^2 LEEM image of the island in (a), showing its faceted structure. The deposition temperature was 530 °C.

overall Ge3*d* intensities, as shown by the shadowed curves in Figs. 2(b) and 2(c). The latter are used to calculate the experimental ratios r_{Ge}.

The same procedure is applied to the images taken at the Si2*p* core-level energies. Figure 2(d) displays the Si2*p* micrograph of the same structure as in Fig. 2(a). It clearly shows a dark island on a bright WL, i.e., an inverted contrast with respect to the Ge3*d* core-level images in Fig. 2(a). This provides further evidence of a Ge enrichment of the topmost layers of the islands, relative to the WL stoichiometry. The Si2*p* spectra are processed through the steps illustrated for the Ge3*d* spectra, resulting in a value for r_{Si} (not shown here). Finally, Eq. (7) allows us to calculate the Si concentration at the island surface. In the present case, we obtained $C_{\mathrm{Si}}{}^{i}=(10\pm3)\%$.

Figure 2(e) displays a LEEM image of the 3D structure in Figs. 2(a) and 2(d), showing the hexagonally shaped base perimeter of the island. Its side facets are oriented along the crystallographic directions of the substrate.

The subtraction of the background from the overall photoelectron intensities represents a crucial step in the described procedure. Figure 3 clearly proves the importance of accurately isolating the selected photoelectron signal out of the measured spectrum. This is remarkably true in the case of the elastic Si2*p* peak, whose signal-to-background ratio may be as small as 1/10. Figure 3 displays the common behavior of the grown islands. A spatially resolved integration of the raw Si2*p* spectra, as in Fig. 3(c), leads to images featuring a brighter center with respect to the periphery of the individual islands. A close inspection of the nature of the detected intensity reveals that the brighter areas in the island images do not stem from a higher Si2*p* signal but rather from the higher background intensity at kinetic energies corresponding to the

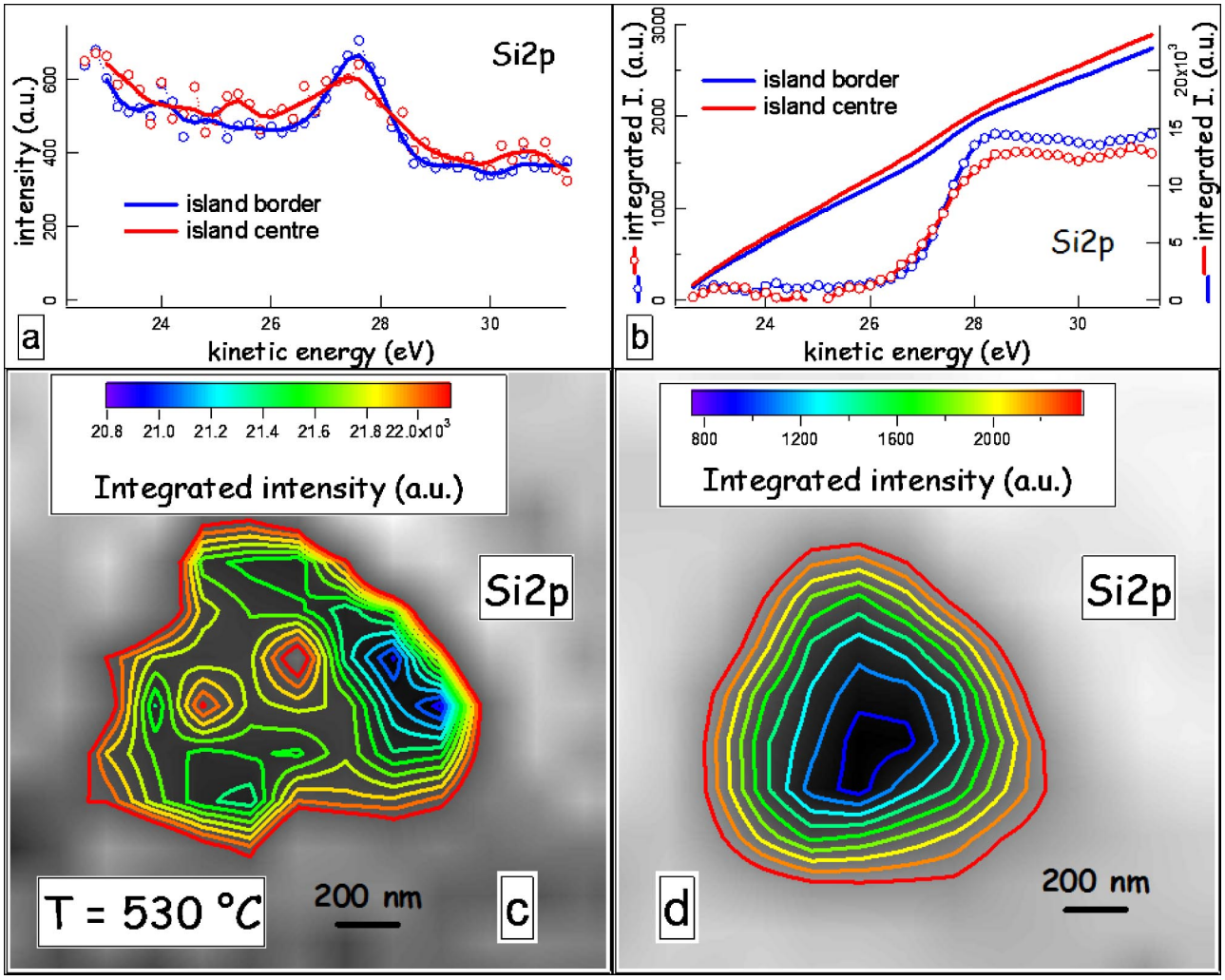

FIG. 3. (Color online) Detailed analysis of the Si2*p* spectrum of the same island as shown in Fig. 2: (a) representative spectra measured at the island border (blue) and center (red); (b) integrated intensities showing the typical contrast within the island surface: the overall raw yields (unbroken lines) are higher at the island center rather than at the border; after background subtraction and integration (circles) the overall Si2*p* signal yields display the opposite trend; (c) 2×2-μm^2 XPEEM raw Si2*p*-integrated image (obtained by summing over the micrographs acquired within a range of photoelectrons energies including the Si2*p* peak): the island center looks brighter than the periphery; and (d) 2×2-μm^2 XPEEM Si2*p* image resulting from background subtraction and consecutive integration (determined by first isolating the elastic contributions and then summing over the images sequence): we note that, despite the rather poor resolution, the center now appears dimmer than the borders. The deposition temperature was 530 °C.

Si2*p* peak [see Figs. 3(a) and 3(b)]. Since the background yield at such energies is mainly due to inelastically scattered Ge3*d* photoelectrons, this is actually consistent with a higher Ge content at the island centers. After background subtraction and integration over the elastic Si2*p* photoelectrons, the contrast in the relevant image, e.g., in Fig. 3(d), is inverted with respect to the raw micrograph in Fig. 3(c). This provides definite proof of Si enrichment at the island borders with respect to the center. This picture is consistent with alloying models based on kinetic considerations and, therefore, on the overwhelming importance of surface, as opposed to bulk, diffusion phenomena.[7,14,16,17] Nevertheless, unraveling the nature of the intermixing processes requires a detailed chemical composition mapping within single islands, which is presently beyond the resolution available.

We emphasize that the visual inspection of the raw data may be misleading and suggest a qualitative picture of the concentration profiles that does not correspond to the correct interpretation of the measurements. In our case, it may lead to the imprudent conclusion that the island centers contain more Si than the edges. This would support bulk diffusion-mediated intermixing models, according to which alloying occurs through defect migration so as to minimize the strain in the system.[14,15,27]

Owing to the limited lateral resolution, the following will focus only on surface concentrations averaged over the upper base of individual three-dimensional structures.

IV. RESULTS

We performed the analysis described in Sec. III for several islands from samples obtained by depositing Ge at different substrate temperatures. At each growth temperature, the acquired LEEM images revealed the coexistence of islands with different geometrical features. Figures 4 and 5, acquired at deposition temperatures of 460 and 530 °C, respectively, show examples of individual 3D structures at different stages of evolution. The smallest islands typically dis-

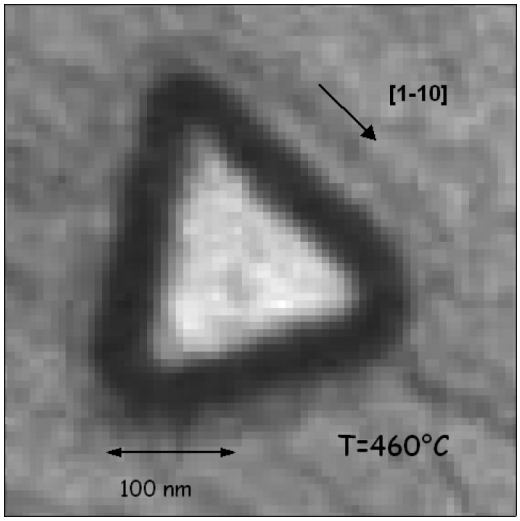

FIG. 4. 500×500-nm^2 LEEM image of a typical triangular island acquired from a sample grown at 460 °C. Note that the regular structure of the facets that bound the island does not seem to be affected by the steps visible on the WL.

play the shape of a truncated pyramid, with a triangular base, which evolves into a more asymmetric-faceted configuration upon further growth. The largest structures generally exhibit a complex-rounded shape and often an atoll-like morphology, i.e., a mass depletion at the island center. In some cases, such mass depletion results in the exposure of the WL.[28] Atoll-like structures are clearly highlighted in LEEM images by the presence of steep concentric contours inside the upper base of the islands.

Figure 6 summarizes the results we obtained by applying the procedure illustrated in Fig. 2. Here, the Si surface content in individual islands is related to their base area. The inset in Fig. 6, taken at a deposition temperature of 530 °C, demonstrates the coexistence of structures at different stages of evolution on the same sample. The experimental points in Fig. 6 clearly show that the 3D structures with a larger area

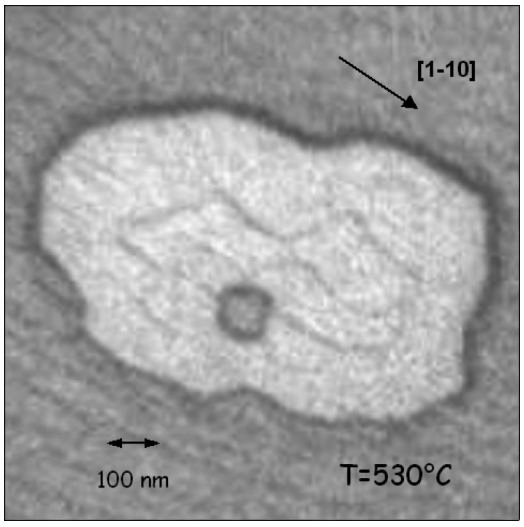

FIG. 5. 1×1-μm^2 LEEM image displaying an example of the largest observed islands, from a sample grown at 530 °C. The atoll-like morphology is clearly visible with an asymmetric depletion that seems to expose an inner portion of the WL.

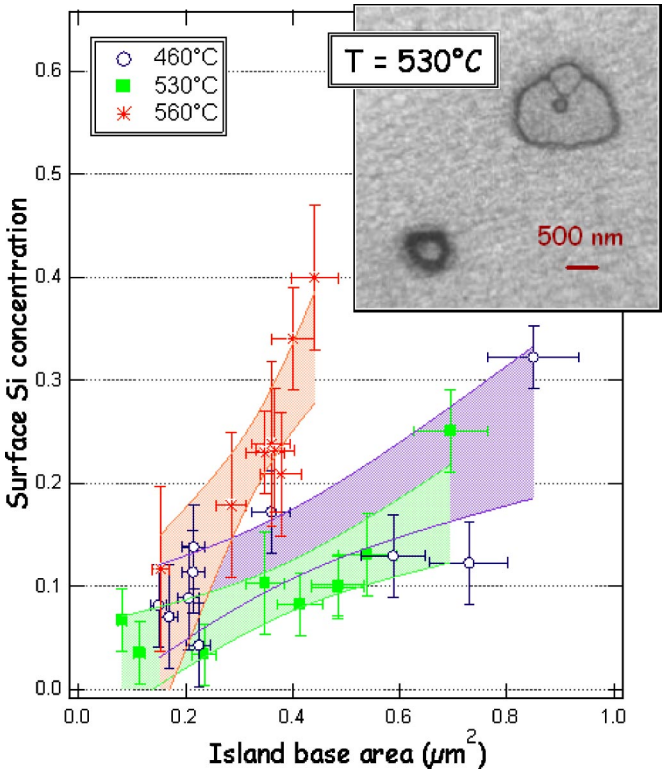

FIG. 6. (Color online) Silicon surface concentration for selected islands vs their basal areas plotted with 90% confidence bands. Islands were grown at the indicated temperatures. Note that the 460 and 530 °C confidence bands overlap over the entire accessed range. Inset: 4.5×4.5-μm^2 LEEM image of a sample grown at 530 °C. Ripened atoll-like structures coexist with smaller islands.

also exhibit a higher surface Si content. The error bars reflect the low signal-to-background ratio, which limits our ability to accurately extract the elastic contributions out of the photoelectron spectra. Nevertheless, the 90% confidence bands superimposed onto the data points suggest that at each deposition temperature, a monotonic relation between the Si concentration in the topmost layers and the basal area of the 3D islands can be established.[29] The smallest and most regularly shaped structures exhibit a Si surface content typically lower than 25%, while their ripening proceeds via an enlargement of their lateral dimensions and the simultaneous increase of C_{Si}^{i} to up to 40%.

A description of a single island ripening through a change in morphological features, from regularly shaped to atoll-like, has already been reported in the literature.[30–32] Our data show that it can also be related to a variation in chemical composition. This is consistent with the observation that an increase in the Si content is generally a necessary condition for the enlargement of the contact area between the WL and the emerging structures, at least until misfit dislocations appear.[12,31,33,34] Our results are qualitatively consistent with Raman-scattering measurements performed on micrometer-sized Ge/Si islands on Si(001) mesas, which displayed comparable features.[35] On the computational side, Monte Carlo simulations were shown to predict a relationship analogous to the one we have reported for the very first stages of island evolution.[36] Figure 6 demonstrates that the stoichiometry or the geometric characteristics of individual islands may be

thought of as equivalent parameters in the description of the ripening stage, at each given deposition temperature.[37–39] Moreover, we note that our results quantitatively support the segregation of Ge at the topmost layers of the islands that we inferred from the contrast in XPEEM images. Indeed the measured $C_{\mathrm{Si}}{}^{i}$ values always remain lower than the 50% Si content reported for the WL.[40,41] This observation agrees with theoretical models, which predict that the element with the largest mismatch component (i.e., Ge in this case, since the in-plane lattice parameters are in registry with the substrate) will segregate into 3D clusters during heteroepitaxial growth.[42,43]

The substrate temperature during Ge deposition strongly influences the slope of the surface concentration—base area correlation. The 90% confidence bands superimposed on the raw data in Fig. 6 show that, while the samples grown at 460 and 530 °C display similar features, dramatic variations are found at 560 °C. Under these growth conditions, the Si surface content increases much more rapidly with the lateral dimensions than at the lower temperatures. Owing to the temperature dependence, the phenomenon must originate from kinetic processes. Yet, the nature and interplay of contributing factors are not thoroughly understood. According to alternative interdiffusion models, Si atoms may be predominantly incorporated into the WL and the 3D islands through their surface mobility,[7,14] through an exchange mechanism involving the bulk,[15] or both. To establish whether the driving force for intermixing is provided by surface kinetic phenomena only or by the tendency to minimize the total strain energy in the islands via a substantial mass exchange with the buried layers, a complete 3D concentration mapping is probably necessary. Surface diffusion alone, which is mainly driven by the entropy, should result in a maximum intermixing located at the peripheries of the islands,[7,14] while an optimum strain relaxation would be attained by increasing the Si content at the cores,[14,15] requiring the exchange of Si and Ge atoms in the bulk.[44,45] At low deposition temperatures the first mechanism should be dominant due to the smaller size of the relevant potential barriers,[46] but at high enough temperatures bulk mass exchange may start to play a significant role. The sudden increase in the slope of the reported curves at 560 °C may be consistent with a thermal switching of the main diffusion phenomena occurring between 530 and 560 °C. At the same time, increasing the temperature may be responsible for the earlier appearance of dislocations, which would allow relatively small islands to relax the strain and exhibit a lower aspect ratio.[47,48] This could be achieved by a temperature-accelerated erosion of the generally Ge-rich island apex, which represents a step towards the development of atoll-like morphologies. The evolution of the process would gradually expose the layers beneath the apex, where the Si content may be enhanced by bulk exchanges. Thus, our results can be interpreted as the complex interaction of different thermally activated processes. To this end, further experimental evidence and sophisticated modeling are needed.

Future developments of the outlined experimental and analytical approach will aim at providing a detailed mapping of the relative Ge/Si stoichiometry at the surface of individual islands grown at different temperatures. This will lead to the identification of the nature of the dominant diffusion phenomena that lead to intermixing in this system.

V. CONCLUSIONS AND OUTLOOK

We have shown that a quantitative measurement of the lateral concentration gradient in 3D islands resulting from the SK growth of Ge on Si(111) can be obtained through an adequate analysis of a set of XPEEM images and spectra. The application of the theoretical framework we have developed may allow a detailed 2D top view stoichiometry mapping of the studied systems, which would yield complementary information with respect to cross-sectional techniques. Our present lateral resolution has allowed us to extract average concentrations from the topmost layers of Ge/Si self-assembled islands. This in turn yields a remarkably rich wealth of information. We have estimated the Si surface content in sets of 3D structures grown at 460, 530, and 560 °C, establishing a correlation between the degree of intermixing and morphological features. As a rule of thumb, the larger the base area of individual islands, the higher the Si concentration in their topmost surface layers, suggesting that both parameters can be used to describe their stages of evolution. We observed that the surface Si content in less-ripened islands is generally less than 25%, while it can increase to 40% in ripened atoll-like structures. The deposition temperature plays a critical role in determining the characteristics of the established relationship between surface composition and lateral dimensions. Thus, our results clearly demonstrate that the intermixing processes are governed by the interplay of different kinetic factors.

Future developments of our experimental activity will aim at pushing further the limits of the present lateral resolution, so as to provide a concentration mapping *within* the surface of individual islands. This is expected to yield a real breakthrough in the comprehension of the diffusion dynamics, leading to alloying at the atomic level.

ACKNOWLEDGMENTS

This work was partially supported by the European Community (EC) through FORUM-FIB Contract No. (IST-2000-29573). One of the authors (F.Ra.) is grateful to the International Council for Canadian Studies for a graduate fellowship. Another author (F.Ro.) acknowledges support from INRS start-up funds, NSERC of Canada, and salary support from FQRNT and the Canada Research Chairs program. We thank R. Paynter for a critical reading of the manuscript and M. Pasqualetto for technical assistance.

[1] T. I. Kamins, E. C. Carr, R. S. Williams, and S. J. Rosner, J. Appl. Phys. **81**, 211 (1997).
[2] F. Rosei, J. Phys.: Condens. Matter **16**, 1373 (2004).
[3] C. Teichert, Phys. Rep. **365**, 335 (2002).
[4] R. Gunella, P. Castrucci, N. Pinto, I. Diavoli, D. Sébilleau, and M. De Crescenzi, Phys. Rev. B **54**, 8882 (1996).
[5] X. R. Qin, B. S. Swartzentruber, and M. G. Lagally, Phys. Rev. Lett. **85**, 3660 (2000).
[6] H. H. Cheng, C. T. Chia, V. A. Markov, X. J. Guo, C. C. Chen, Y. H. Peng, and C. H. Kuan, Thin Solid Films **369**, 182 (2000).
[7] N. Liu, J. Tersoff, O. Baklenov, A. L. Holmes Jr., and C. K. Shih, Phys.

Rev. Lett. **84**, 334 (2000).
[8]TEM was used to evaluate concentration profiles in combination with several techniques, such as electron-energy-loss spectroscopy (EELS) (see Refs. 9–11), energy dispersive x-ray microanalysis (EDX) (see Ref. 12), or even just taking advantage of Vegard's law (see Ref. 13), which projects a linear dependence of the average lattice parameters on atomic fractions in an alloy.
[9]Y. Zhang, M. Floyd, K. P. Driver, J. Drucker, P. A. Crozier, and D. J. Smith, Appl. Phys. Lett. **80**, 3623 (2002).
[10]T. Walther, C. J. Humphreys, and A. G. Cullis, Appl. Phys. Lett. **71**, 809 (1997).
[11]X. Z. Liao, J. Zou, D. J. H. Cockayne, J. Qin, Z. M. Jiang, X. Wang, and R. Leon, Phys. Rev. B **60**, 15605 (1999).
[12]X. Z. Liao, J. Zou, D. J. H. Cockayne, Z. M. Jiang, X. Wang, and R. Leon, Appl. Phys. Lett. **77**, 1304 (2000).
[13]A. Rosenauer, U. Fisher, D. Gerthsen, and A. Förster, Appl. Phys. Lett. **71**, 3868 (1997).
[14]U. Denker, M. Stoffel, and O. G. Schmidt, Phys. Rev. Lett. **90**, 196102 (2003).
[15]A. Malachias, S. Kycia, G. Medeiros-Ribeiro, R. Magalhães-Paniago, T. I. Kamins, and R. S. Williams, Phys. Rev. Lett. **91**, 176101 (2003).
[16]S. W. Lee, L. J. Chen, P. S. Chen, M. J. Tsai, C. W. Liu, T. Y. Chien, and C. T. Chia, Appl. Phys. Lett. **83**, 5283 (2003).
[17]T. Ide, A. Sakai, and K. Shimizu, Thin Solid Films **357**, 22 (1999).
[18]F. Ratto, F. Rosei, A. Locatelli, S. Cherifi, S. Fontana, S. Heun, P. D. Szkutnik, A. Sgarlata, M. De Crescenzi, and N. Motta, Appl. Phys. Lett. **84**, 4526 (2004).
[19]Th. Schmidt, S. Heun, J. Slezak, J. Diaz, K. C. Prince, G. Lilienkamp, and E. Bauer, Surf. Rev. Lett. **5**, 1287 (1998).
[20]A. Locatelli, A. Bianco, D. Cocco, S. Cherifi, S. Heun, M. Marsi, M. Pasqualetto, and E. Bauer, J. Phys. IV **104**, 99 (2003).
[21]http://www.elettra.trieste.it/experiments/beamlines/nano/index.html
[22]R. M. Tromp, F. M. Ross, and M. C. Reuter, Phys. Rev. Lett. **84**, 4641 (2000).
[23]P. Sutter, E. Mateeva, J. S. Sullivan, and M. G. Lagally, Thin Solid Films **336**, 262 (1998).
[24]Since it is very well established that the phase transition occurs at 830 °C, it was used as a reference to calibrate the thermocouple employed for sample temperature reading.
[25]G. Capellini, M. De Seta, and F. Evangelisti, Appl. Phys. Lett. **78**, 303 (2001).
[26]S. Tanuma, C. J. Powell, and D. R. Penn, Surf. Interface Anal. **17**, 911 (1991).
[27]S. A. Chaparro, J. Drucker, Y. Zhang, D. Chandrasekhar, M. R. McCartney, and D. J. Smith, Phys. Rev. Lett. **83**, 1199 (1999).
[28]The central part of such ripened islands was not analyzed by means of the described XPEEM procedure, since some of our assumptions may fail there [see the discussion following Eq. (3)].
[29]The data points were fitted using a linear regression. The confidence bands enclose the region over which lines may span up to a probability of 90% and demonstrate that the slope is positive within a 90% confidence interval.
[30]F. Boscherini, G. Capellini, L. Di Gaspare, M. De Seta, F. Rosei, A. Sgarlata, N. Motta, and S. Mobilio, Thin Solid Films **380**, 173 (2000).
[31]N. Motta, A. Sgarlata, R. Calarco, J. Castro Cal, F. Patella, A. Balzarotti, and M. De Crescenzi, Surf. Sci. **406**, 254 (1998).
[32]G. Capellini, N. Motta, A. Sgarlata, and R. Calarco, Solid State Commun. **112**, 145 (1999).
[33]J. Drucker, Y. Zhang, S. A. Chaparro, D. Chandrasekhar, M. R. McCartney, and D. J. Smith, Surf. Rev. Lett. **7**, 527 (2000).
[34]J. A. Floro, E. Chason, R. D. Twesten, R. Q. Hwang, and L. B. Freund, Phys. Rev. Lett. **79**, 3946 (1997).
[35]D. V. Regelman, V. Magidson, R. Beserman, and K. Dettmer, Thin Solid Films **336**, 73 (1998).
[36]P. C. Kelires, J. Phys.: Condens. Matter **16**, 1485 (2004).
[37]Intermixing was already reported to influence the overall geometrical features of statistical ensembles of Ge/Si islands grown on Si(001) and to promote an enlargement of their lateral dimensions (see Refs. 38 and 39).
[38]T. I. Kamins, G. Medeiros-Ribeiro, D. A. A. Ohlberg, and R. S. Williams, Appl. Phys. A: Mater. Sci. Process. **67**, 727 (1998).
[39]W. L. Henstrom, C. P. Liu, J. M. Gibson, T. I. Kamins, and R. S. Williams, Appl. Phys. Lett. **77**, 1623 (2000).
[40]K. Tillmann and W. Jäger, J. Electron Microsc. **49**, 245 (2000).
[41]F. Boscherini, G. Capellini, L. Di Gaspare, F. Rosei, N. Motta, and S. Mobilio, Appl. Phys. Lett. **76**, 682 (2000).
[42]D. B. Migas, P. Raiteri, L. Miglio, A. Rastelli, and H. von Känel, Phys. Rev. B **69**, 235318 (2004).
[43]J. Tersoff, Phys. Rev. Lett. **81**, 3183 (1998).
[44]Numerical simulations were performed based on atomic identity flipping with an adequate potential modeling and the assumption that interdiffusion does not occur during growth (see Ref. 45).
[45]P. Sonnet and P. C. Kelires, Phys. Rev. B **66**, 205307 (2002).
[46]R. J. Wagner and E. Gulari, Phys. Rev. B **69**, 195312 (2004).
[47]J. Walz, A. Greuer, G. Wedler, T. Hesjedal, E. Chilla, and R. Koch, Appl. Phys. Lett. **73**, 2579 (1998).
[48]G. Wedler, J. Walz, T. Hesjedal, E. Chilla, and R. Koch, Phys. Rev. Lett. **80**, 2382 (1998).